RSC Advances

ROYAL SOCIETY OF CHEMISTRY

www.rsc.org/advances

TABLE OF CONTENTS

Zinc oxide quantum dots show increasing emission intensities and decreasing band gaps upon size reduction promoted by organosilane functionalization.

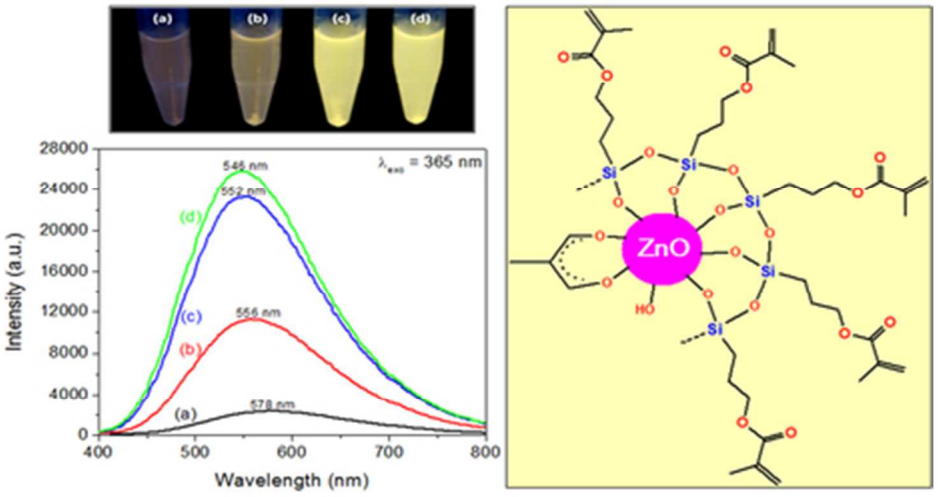

39x26mm (300 x 300 DPI)

Cite this: DOI: 10.1039/c0xx00000x

www.rsc.org/xxxxxx

ARTICLE TYPE

Size-dependent photoluminescence of zinc oxide quantum dots through organosilane functionalization

Viorica Mușat,*[a] Aurel Tăbăcaru,[a] Bogdan Ștefan Vasile[b] and Vasile-Adrian Surdu[b]

Received (in XXX, XXX) Xth XXXXXXXXX 20XX, Accepted Xth XXXXXXXXX 20XX

DOI: 10.1039/b000000x

Organosilane grafting on ZnO nanoparticles surface constitutes an appealing route towards the fabrication of hybrid nanomaterials with tuned optical and physico-chemical properties. In this paper the synthesis, morpho-structural characterization and optical properties of hybrid ZnO quantum dots (QDs) grafted with variable amount (2, 5 to 10 % of Si/Zn molar ratio) of 3-(trimethoxysilyl)propylmethacrylate (MPS) surfactant are reported. The organosilane surfactant was chosen to evaluate the ability of both preventing nanoparticles agglomeration and tuning the optical properties of the resulting hybrid nanomaterials. The grafted ZnO QDs were prepared through a modified precipitation method and their characterization was performed by means of X-ray diffraction (XRD), High-resolution Transmission Electron Microscopy (HRTEM), Fourier Transform Infrared spectroscopy (FTIR), Thermogravimetric analysis (TGA), while their optical properties were studied by UV-VIS spectroscopy. Unmodified ZnO and MPS-grafted ZnO QDs showed optical transmittance between 85 and 90%, and low reflectance in the visible domain, while a significant blue-shift of the photoemission bands was observed passing from 578 nm for unmodified ZnO to 546 nm for ZnO grafted with MPS 10%. This shift can be associated to the size reduction of ZnO QDs upon increasing amount of MPS. A decrease of band gap energies, considering the effect of organosilane surfactant on the nanoparticles size reduction, from 3.494 eV for unmodified ZnO to 3.377 eV for ZnO-MPS 10% was for the first time detected and discussed, giving a new insight into the relationship between the nanoparticle size reduction promoted by an organic surfactant with electron injection into ZnO bands and the value of band gap energy.

1. Introduction

ZnO nanoparticles are continuously gaining ground of scientific research, reaching a high character of multidisplinarity and demonstrating their utility in various potential applications, *e.g.*, optics, electronics, optoelectronics (*i.e.* light emitting diodes), UV lasers and photodetectors,[1] solar cells,[2] and thin film transistors (TFTs).[3] Over the years, this metal oxide semiconductor with a wide bandgap (3.37 eV) and high exciton binding energy (60 meV) at room temperature, has also been investigated in many other interesting applications, such as gas sensing,[4] catalysis,[5] cell labeling,[6] and as antifouling,[7] photocatalytic and antibacterial[8] agents.

Many of the above mentioned applications require the control of the properties of the nanoparticles surface. In particular, optical and optoelectonical properties are essentially dependent on the nanoparticle size. A crucial shortcoming that may arise when adopting oxide nanoparticles in view of practical applications is their tendency to agglomerate, thus making more difficult to take advantage of their utilization in the form of very small nanoparticles, and therefore, it is of great importance to have a better control over their particles size and surface properties. In the light of this, stabilization through organic functionalization of ZnO surface nanoparticles is a useful strategy for controlling and, eventually, suppressing their agglomeration, growth and surface defects.[9,10] As a matter of fact, by applying this strategic surface grafting, it is possible to attain a significant reduction of the particles size to the level of quantum dots, thus allowing to tune the optical, photoluminescent and physico-chemical properties. In this respect, several reports dealing with ZnO surface grafting with different organic species such as thiols,[10] polymers[11] and alkylamines,[12] have started to address this recent and useful trend of surface modification.

Considering the importance of surface organo-modification, herein we turn our attention to one promissing representative of the organosilanes class, namely the 3-(trimethoxysilyl)propylmethacrylate (MPS). Its reactive alkoxy functional groups can provide strong and stable chemical bonds with inorganic species upon hydrolysis followed by condensation reactions. Despite this useful reactivity towards surface modification, only few reports have described so far the synthesis of MPS-grafted ZnO nanoparticles along with a detailed NMR spectroscopic characterization of the structural organization of hydrolyzed MPS molecules onto the ZnO surface.[13,14] Incorporation of very small number of organic surfactant-grafted ZnO nanoparticles into transparent nanocomposite films for the study of optical and photoluminescent properties can also be found in the literature.[15,16]

Recognizing the great potentiality of MPS species to establish stable covalent bonds upon ZnO surface grafting, with direct influence on its structure, morphology and electronic features, we sought to obtain and morpho-structurally characterize a new series of MPS-grafted ZnO QDs using different Zn/Si molar ratios (i.e., 2, 5 and 10%, respectively). A systematic study of still

unexplored optical properties on this series such as, *e.g.,* transmittance, reflectance and photoluminescence, is also undertaken. The choice of this type of organosilane surfactant is part of our strategy to explore the tuning of optical properties taking into account the nature of end group bound to silicon. Moreover, silicon-based species are known to ensure upon hydrolysis very good cohesion and adhesion when deposited as films or layers on rigid or flexible substrates in order to achieve, *e.g.*, hybrid light emitting devices (HLEDs) with high stability and transparency.[17]

Their syntheses were conducted through a simple and non-expensive modified precipitation method, while their characterization was performed by means of X-ray diffraction (XRD), high-resolution trasmission electron microscopy (HRTEM), Fourier Transform Infrared spectroscopy (FTIR), thermogravimetric analysis (TGA) and elemental analysis. The effect of variable concentration of MPS surfactant on the optical properties was also investigated. An unexpected decrease of band gap energy, compared with the well known effect of nanoparticles size reduction was obtained, and thus giving a new insight into the relationship between the value of band gap energy and the nature of the organic surfactant that promoted the nanoparticle size reduction.

2. Experimental Section

2.1 Materials and synthesis of ZnO QDs

Zinc acetate dihydrate (purity >98%), methanol, 3-(trimethoxysilyl)propylmethacrylate (purity = 98%) and potassium hydroxide were purchased from Sigma Aldrich and used without further purification.

ZnO QDs were synthesized according to a sligthly modified precipitation method reported in the literature.[13] For the sake of completeness the detailed synthetic procedure is given in the Supporting Information. The obtained samples are hereafter labeled with ZnO-MPS x%, where x = 2, 5 and 10, respectively, is the Si/Zn molar ratio used in the synthesis, whereas the reference sample prepared without organic silane is simply labeled with ZnO.

2.2 Characterization methods

X-ray diffraction (XRD) patterns were recorded on ground powders with an Empyrean (PANalytical, the Netherlands) diffractometer using a Cu $K_{\alpha 1}$ (λ = 1.540598) radiation, equiped with 2xGe(220) hybrid monochromator for Cu and PIXcel3D detector. The analyses were performed by using Bragg-Brentano geometry ("theta-2theta") for angles between 10 and 80° 2θ degrees with a step size of 0.04° and acquisition time on step size of 3 s. Sample preparation: a small amount of each sample was mounted on a single crystal silicon holder, which does not give diffraction interferences in the analysis range for the radiation emitted by a Cu anode. The sample was gently pressed on the holder so that the analyzed area be flat. For the identification of cell parameters and mean crystallite size, Rietveld refinement was performed. The acceptance indexes considered for the refinement are $R_{expected}$, $R_{profile}$, Weighted R profile and Goodness of fit, respectively. In Table S1 (Supporting Information) relevant crystallografic data for unmodified and MPS-modified ZnO nanoparticles are provided.

The transmission electron microscopy images were obtained on finely powdered samples using a Tecnai™ G2 F30 S-TWIN high resolution transmission electron microscope (HRTEM) from FEI. The microscope was operated in transmission mode at 300 kV with TEM point resolution of 2 Å and line resolution of 1 Å. The finely ZnO powders were dispersed into pure ethanol and ultrasonicated for 15 min. After that diluted sample was put onto a holey carbon coated copper grid and left to dry before it was analyzed through TEM.

Fourier Transform Infrared spectra (FTIR) were recorded from 4000 to 650 cm^{-1} with a Perkin-Elmer Spectrum 100 instrument by total reflectance on a ZnSe crystal (resolution of 4 cm^{-1}).

The elemental analyses (C, H) were performed with a Fisons Instruments 1108 CHNS-O Elemental Analyzer. Before performing these analyses, all the samples were dried *in vacuum* (50 °C, ~ 0.1 Torr) till a constant weight was reached.

Thermogravimetric analysis (TGA) were performed under pure air atmosphere (gas flow 25 mL/min) with a TA Instruments TGA Q5000, heating the samples from room temperature to 700 °C at a heating rate of 5 °C/min.

The optical transmission and reflectance spectra were acquired at room temperature with a Perkin Elmer (Lambda 35) UV-VIS-NIR spectrophotometer, operated in air, at normal incidence, in the 190 – 1100 nm spectral range. Specimens were prepared by dispersing the obtained nanoparticles by sonication in isopropanol and depositing as thin films on glass substrate by spin coating (2000 rpm, 20s). The optical band gap energy, E_g, was estimated from the fundamental absorption edge of the nanoparticles-based thin films, assuming a direct transition between valence and conduction band. The values of optical band gap were determined from the dependency of absorption coefficient, α, on the photon energy, $h\nu$, given by equation (1):

$$(\alpha h\nu)^2 = A(h\nu - E_g) \quad (1)$$

where A is a parameter that depends on the transition probability.[18-25] The absorption coefficient, α, was calculated by equation (2):

$$\alpha = \frac{1}{d}\ln\left[\frac{(1-R)^2 + \sqrt{(1-R)^2 + 4R^2T^2}}{2T}\right] \quad (2)$$

where d is the film thickness, T is the transmittance and R reflectance of the investigated samples.[26-29]

The thickness of the deposed thin films was determined by means of MII-4 interference microscope (type Linnik) with an error not exceeding 0.01 μm, using multiple-beam Fizeau fringe method.[30] The thickness of the thin films was determined to be *ca.* 258 nm.

The solid state photoluminescence emission spectra were recorded at room temperature with a Perkin-Elmer LS 45 Luminescence Spectrometer equipped with a pulsed Xe flash lamp. The photoluminescence spectra recorded in the range 400-800 nm range were collected for an optimal excitation wavelength of 365 nm, where the emission responses in the case of all samples were found to be the most intense.

3. Results and Discussion

3.1 Structure and morphology

The XRD patterns of all samples (Figure 1) show the main diffraction peaks located at 31.6, 34.4, 36.1, 47.4, 56.4, 62.6 and 67.9° 2θ, assignable to the (100), (002), (101), (102), (110), (103) and (112) planes, respectively, of wurzite structure of zinc oxide.[31] An observation regarding the intensity and full width at half maximum (FWHM) of main diffraction peaks, while passing from unmodified ZnO to maximum loaded MPS-grafted ZnO QDs, highlights the significant effect of MPS grafting on the structure of zinc oxide nanoparticles. As such, the XRD pattern of unmodified ZnO displays well resolved reflections, while a progressive broadening of the diffraction peaks can be observed in the case of ZnO-MPS 2%, ZnO-MPS 5% and ZnO-MPS 10%,

respectively. This might be resulted from the size reduction effects induced through organic silane functionalization along with a reduction of crystallinity.

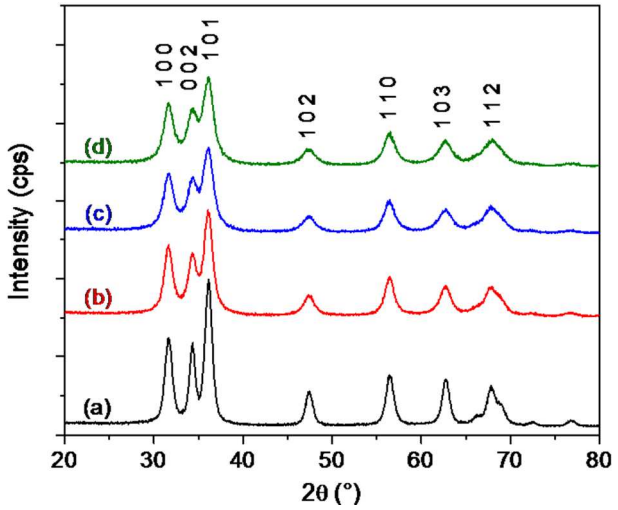

Figure 1. XRD profiles of ZnO (a), ZnO-MPS 2% (b), ZnO-MPS 5% (c) and ZnO-MPS 10% (d).

The average crystallite size (L) of synthesized ZnO QDs was estimated by applying the Debye-Scherrer's equation, $B(2\theta) = (K\cdot\lambda)/(L\cdot\cos\theta)$ to the (100), (102) and (110) planes, where B is the full width at half of the maximum intensity (FWHM), λ is the X-ray wavelength, θ is the diffraction angle and K is the Scherrer's constant whose value for spherical particles is 0.89.[32] A progressive decrease of the estimated crystallite size passing from 7.57 nm for unmodified ZnO QDs to 5.24, 4.34 and 4.19 nm for ZnO QDs grafted with 2, 5 and 10%, respectively, was evidenced.

High resolution transmission electron microscopy (HRTEM) was employed to assess the average particles size and morphology of ZnO samples, and their micrographs along with the corresponding histograms are given in Figure 2. The selected area electron diffraction (SAED) patterns of ZnO QDs were also determined, and the corresponding results are shown in Figure S1 (Supporting Information). All the diffraction rings were attributed to ZnO featuring the wurtzite structure in line with the XRD data. HRTEM image of unmodified ZnO QDs (Fig. 2A) reveals nearly spherical or ellipsoidal shapes. As indicated by the histogram reported in Fig. 2A' (determined by measuring the diameter of more than one hundred ZnO nanocrystals) the unmodified ZnO QDs are characterized by particle size distribution centered at 10.67±0.29 nm, which is slightly higher than the average size estimated from XRD data. Quantum dots with similar morphology can be discerned for all the organosilane-based ZnO samples. Their HRTEM micrographs show that passing from unmodified ZnO to organo-modified ZnO QDs the size undergoes a significant decrease (about half) for QDs grafted with 2% MPS, while the increase of MPS concentration to 5 and 10%, respectively, produces only small and not significant decreases in nanoparticle size (Fig. 2B-D). Fig. 2B' shows the histogram of ZnO-MPS 2% and the measured average diameter is centered at 4.02±0.21 nm, which is close to the estimated value calculated from XRD data. The histograms of ZnO-MPS 5% and ZnO-MPS 10% (Fig. 2, C' and D') show very close values of the average diameter that are centered at 3.86±0.09 nm and 3.85±0.1 nm, respectively, and are also close to estimated values calculated from XRD data.

In other words, the higher the organosilane concentration is, the smaller ZnO crystallites size and the smaller grafted ZnO QDs are. These results demonstrate that the variable amount of MPS introduced in the synthesis process influences not only the growth of ZnO crystallites, but also the growth of ZnO QDs, leading to obtaining oxide quantum dots. This explains the effect of MPS by its direct participation to the condensation reaction with $Zn(OH)_2$ and ZnO species, and thus, limiting the self-condensation of $Zn(OH)_2$ for the primary ZnO crystallite growth and then along with their agglomeration (Scheme S1, Supporting Information).[13,14]

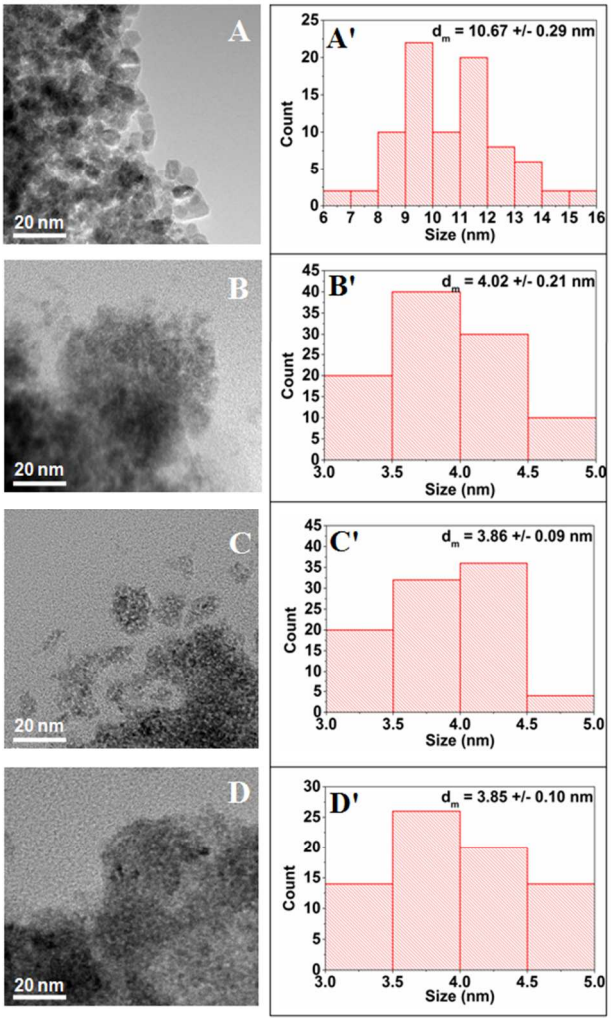

Figure 2. HRTEM micrographs of ZnO (A), ZnO-MPS 2% (B), ZnO-MPS 5% (C) and ZnO-MPS 10% (D); the histograms of the particle size of all samples are displayed in frames A', B', C' and D', respectively.

3.2 FTIR Spectroscopy

FTIR spectroscopy was used to investigate the binding of MPS molecules on the surface of ZnO QDs. The IR spectra of both unmodified ZnO and organosilane-modified ZnO samples, collectively gathered in Figure 3, display a broad band in the 3500-3000 cm^{-1} range that can be assigned to the stretching vibration of OH groups coming from residual physisorbed water on the particles surface. Two strong bands located at 1566 and 1416 cm^{-1} in ZnO, at 1562 and 1420 cm^{-1} in ZnO-MPS 2%, at 1567 and 1408 cm^{-1} in ZnO-MPS 5%, and at 1567 and 1409 cm^{-1}

in ZnO-MPS 10% are assigned to the asymmetric and symmetric stretching modes of carboxylate groups (COO^-) of residual acetate anions chemically attached on the ZnO surface during the synthesis process, difficult to be completely removed upon even intense washing of the samples. Their difference, $\Delta\nu = \nu_a - \nu_s$ = 150 cm^{-1} in ZnO, 142 cm^{-1} in ZnO_MPS 2%, 159 cm^{-1} in ZnO_MPS 5% and 158 cm^{-1} in ZnO_MPS, respectively, most likely indicates a bridging coordination geometry.[33] On the other hand, a decrease in the intensity of the two bands when passing from unmodified ZnO to ZnO-MPS 10% can be observed, due to their (residual carboxylate groups) replacement by MPS molecules. The broad peak at 892 cm^{-1} can be attributed to Zn-OH bonds formed by chemical attachment of the hydroxy groups on the ZnO particles.

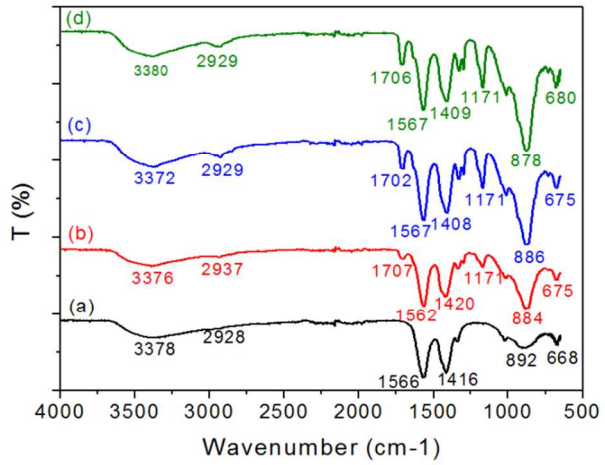

Figure 3. FTIR spectra of ZnO (a), ZnO-MPS 2% (b), ZnO-MPS 5% (c) and ZnO-MPS 10% (d).

In the IR spectrum of free MPS (Figure S2), the bands at 1715, 1637 and 1161 cm^{-1} are assigned to the vibrations of C=O, C=C and C–O bonds, respectively, while in the spectra of MPS-treated ZnO QDs the shift of C=O stretch at 1702-1707 cm^{-1} along with a minor shift of C–O stretch at 1171 cm^{-1} confidently indicate the successful ZnO surface functionalization through chemical bonding. On the other hand, an increase in the intensity of these two specific bands passing from simple ZnO to ZnO_MPS 10% can be observed. Furthermore, the presence of a very weak C=C stretch in the MPS-treated ZnO samples located at 1632-1638 cm^{-1}, partially overlapped with the very strong asymmetric band of carboxylate, may suggest that no network polymerization by cross-linking of the pendant methacrylate end groups takes place. Additional absorbtion bands located at 1075 and 934 cm^{-1} characteristic of Si–O–C bonds in free MPS, completely dissapear in MPS-treated ZnO samples, indicating that condensation between the methyl groups from trimethoxysilane moiety and the hydroxy groups on the ZnO surface has successfully occured.[34]

The bands at 2838 and 2944 cm^{-1} belong to the aliphatic C–H bonds present in the unhydrolized MPS, while in the MPS-grafted ZnO samples the bands observed in the range 2800-3000 cm^{-1} include the vibration stretchings of $-CH_2$ groups of the propyl chain bound to silane moiety on the ZnO surface and also $-CH_3$ groups from both the acetate anions and methacrylate groups. The intense peak at 812 cm^{-1} in the free MPS is characteristic to the symmetric stretching of Si-O-CH_3, while in the MPS-based ZnO samples it dissapears giving rise to the complete reaction between MPS and hydrolyzed ZnO particles. A new finely splitted and very strong band located at 878-884 cm^{-1} that appeared in the MPS-grafted ZnO samples could indicate the formation of both Zn–O–Si bonds during the functionalization process and Si–O–Si bridges formed by a self-condensation of the organosilanes used to modify the ZnO surface.[12] In Figure 4 a sketch of a simplified structural model of organosilane-treated ZnO QDs is proposed, in which the condensed silane moieties give the shape of a cross-linked shell with the methacrylate groups oriented outwardly.

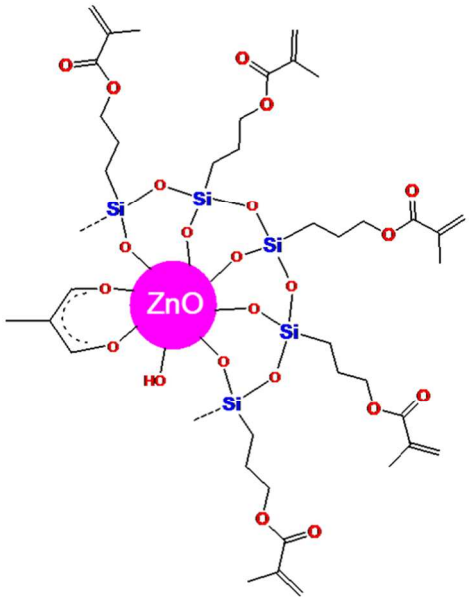

Figure 4. Proposed structural model of the organosilane-treated ZnO nanoparticles.

3.3 Thermogravimetric analysis

The thermal behavior of unmodified and organo-modified ZnO nanoparticles was investigated by thermogravimetric analysis (TGA), in order to assess their thermal stability and to identify the main weight losses occuring in the samples along the heating process. The TGA results (hereafter discussed), FTIR data and Elemental Analyses (C, H) concurred in proposing the stoechiometric formulae of both unmodified ZnO and MPS-treated ZnO samples (Table S1, Supporting Information).

The TGA profile of unmodified ZnO sample (Figure 5A, curve a) shows a first weight loss of 1.51% in the range 30 – 120 °C, due to the evaporation of two physically adsorbed water molecules onto the ZnO surface (theoretical weight loss: 1.53%, in close agreement with the experimental value). A second weight loss of 0.73% in the range 120 – 220 °C can be ascribed to the evolution of one water molecule possibly resulted from two hydroxy groups chemically attached onto the ZnO surface (theoretical weight loss: 0.76%). A third weight loss of 4.61% in the range 220 – 500 °C is due to the decomposition of the acetate anion that may release acetone and carbon dioxide as already proposed by Hiltunen *et al.*[35] (theoretical weight loss: 4.33%). The corresponding DTG curve (Figure 5B, curve a) shows one peak at 53 °C assigned to the evaporation of physisorbed water molecules and one set of peaks at 296, 353 and 374 °C, respectively, assigned to a more complex thermal decomposition of the acetate ions bound to the ZnO surface.

The TGA profile of ZnO-MPS 2% sample (Figure 5A, curve b) shows a first weight loss of 1.18% in the range 30 – 120 °C, due to the evaporation of two physically adsorbed water molecules

onto the ZnO surface (theoretical weight loss: 1.19%, in close agreement with the experimental value). A second weight loss of 1.17% in the range 120 – 220 °C can be ascribed to the evolution of two water molecules resulted from the condensation reaction, promoted by heating, of two zinc(II) hydroxide molecules possibly present in the sample as a trace in very small amount (theoretical weight loss: 1.19%). A further cumulative weight loss of 6.57% in the range 220 – 500 °C can be assigned to the decomposition of both the acetate anion and the demethylated MPS that breaks into one propylmethacrylate ($C_7H_{11}O_3$) fragment and silicon dioxide (theoretical weight: 6.68%). It is well known that the alkoxysilane group releases by thermal decomposition the corresponding silicon dioxide (SiO_2) as detected, for example, by Musat *et al.*,[36] who reported on the thermal studies of sol-gel precursors containing zinc acetate as ZnO source and tetraethoxysilane as SiO_2 source. The corresponding DTG curve (Figure 5B, curve b) shows one peak at 50 °C assigned to the evaporation of physisorbed water molecules and one set of peaks at 314 and 370 °C, respectively, assigned to the thermal decomposition of acetate ions and demethylated MPS bound to the ZnO surface.[14]

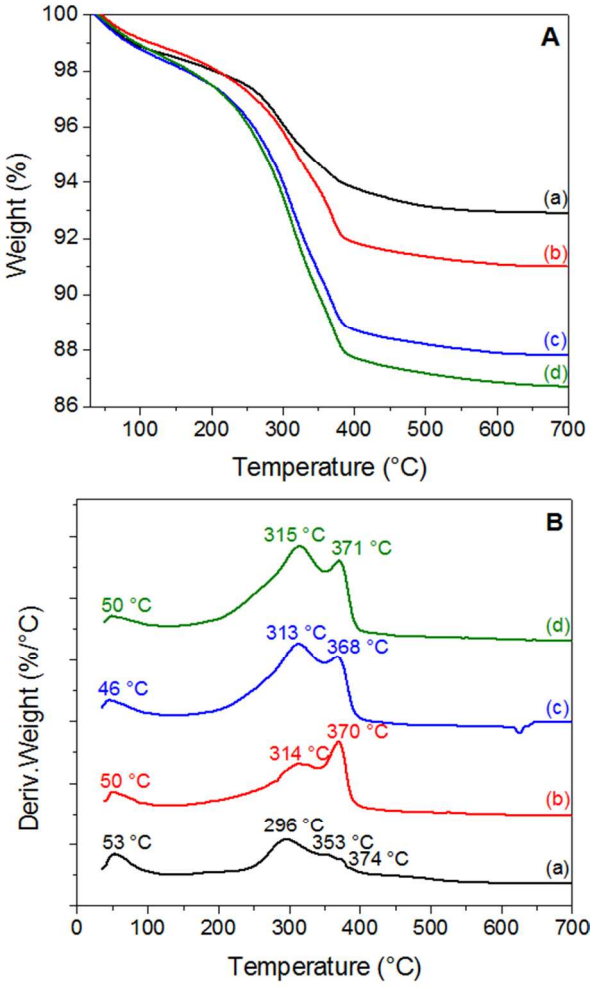

Figure 5. TGA (A) and DTG (B) curves of ZnO (a), ZnO-MPS 2% (b), ZnO-MPS 5% (c) and ZnO-MPS 10% (d).

The TGA profile of ZnO-MPS 5% sample (Figure 5A, curve c) shows a first cumulative weight loss of 2.54% in the range 30 – 200 °C, due to the removal of two physically adsorbed water molecules (1.02%) and three water molecules (1.52%) resulted from the condensation reaction, promoted by heating, of two zinc(II) hydroxide molecules possibly present in the sample as a trace in very small amount (theoretical weight loss: 2.57%). A further cumulative weight loss of 9.67% in the range 220 – 500 °C is due to the decomposition of both the acetate anion and demethylated MPS broken into two propylmethacrylate fragments and silica (theoretical weight loss: 9.85%). The corresponding DTG curve (Figure 5B, curve c) shows one peak at 46 °C assigned to the evaporation of physisorbed water molecules and one set of peaks at 313 and 368 °C, respectively, assigned to the thermal decomposition of acetate ions and demethylated MPS bound to the ZnO surface.[14]

Finally, the TGA profile of ZnO-MPS 10% sample (Figure 5A, curve d) shows a first cumulative weight loss of 3% in the range 30 – 220 °C, due to the removal by evaporation of three physically adsorbed water molecules (1.07%) and five water molecules (1.93%) resulted from the condensation reaction, promoted by heating, of four zinc(II) hydroxide molecules possibly present in the sample as a trace in very small amount (theoretical weight loss: 3.1%). A further cumulative weight loss of 10.27% in the range 220 – 500 °C is due to the decomposition of both the acetate anion and demethylated MPS broken into three propylmethacrylate fragments and silica (theoretical weight loss: 10.86%). The corresponding DTG curve (Figure 5B, curve d) shows one peak at 50 °C assigned to the evaporation of physisorbed water molecules and one set of peaks at 315 and 371 °C, respectively, assigned to the thermal decomposition of acetate ions and demethylated MPS bound to the ZnO surface.[14]

From an overall comparison of these TGA results, it can be observed that all the MPS-grafted ZnO QDs contained a very low amount of physisorbed water molecules lying in the narrowest 1 – 1.2 % range with respect to unmodified ZnO sample, thus suggesting their remarkable hydrophobic character attained upon successful functionalization. As far as their thermal stability is concerned, all samples were found to be stable up to 225 °C as determined by their decomposition onset established around this value.

3.4 Optical properties

Figure 6 presents the optical transmittance and the reflectance spectra in the UV-Vis-NIR wavelength region (200-1100 nm) of the thin films based on unmodified ZnO and organosilane-modified ZnO samples. All these films, with measured thickness of about 258 nm, show between 85 and 90% optical transmittance in the visible range. As compared to unmodified ZnO-based film, a slight increase of optical transmittance of MPS-modified ZnO nanoparticles-based thin films is observed in 400-800 nm range, which is understandable considering the presence of organosilane surfactant that contributes to the transparency of resulted hybrid thin films. The increase of transmittance in the visible domain can also be associated with the decreased size of nanoparticles along with decreased agglomeration.

From Figure 7, one can observe a decrease of the band gap energy of MPS-modified ZnO nanoparticles as compared to unmodified ZnO nanoparticles. A continuous decrease was observed with increasing the MPS concentration, from 3.494 eV for unmodified ZnO nanoparticles to 3.377eV for 10% MPS-modified ZnO nanoparticles. The value of 3.494 eV is consistently higher than the value of 3.37 eV known for bulk ZnO. These high values were also reported for zinc oxide nanostructures.[37] The largest variation of band gap of 0.085 eV (from 3.494 to 3.409eV) was observed when ZnO QDs were grafted with 2% MPS, the latter showing the largest size decrease (by half) relative to the unmodified ZnO. Increasing MPS

concentration from 2 to 5% and from 5 to 10% causes smaller variation of 0.02 eV and 0.01 eV, respectively, in accordance with very little change in the size of nanoparticles (Fig. 2A-D). This nearly exponential decay might be explained by the composition and morphology variation of the films as a function of the grafting concentration.[38]

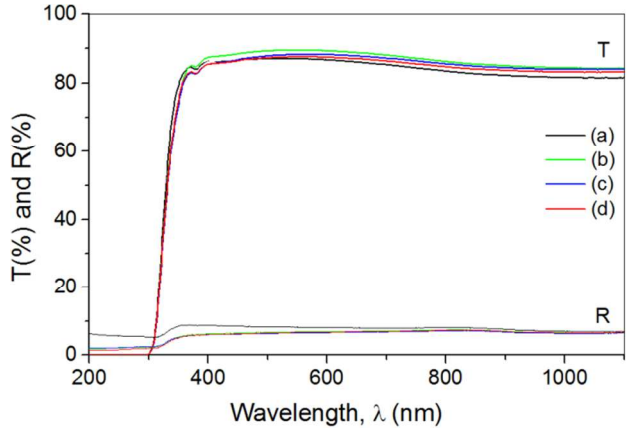

Figure 6. Optical transmittance and reflectance spectra of ZnO (a), ZnO-MPS 2% (b), ZnO-MPS 5% (c) and ZnO-MPS 10% (d).

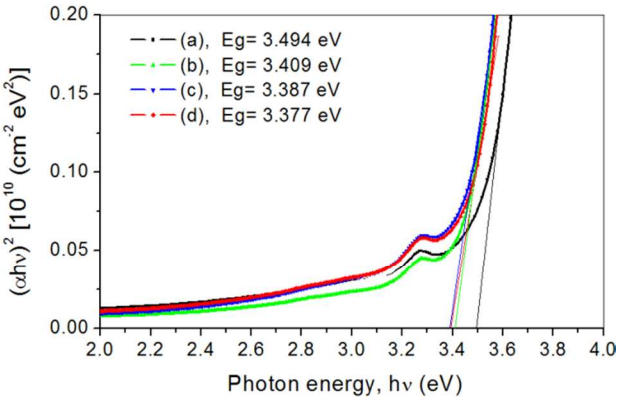

Figure 7. The plots $(\alpha h\upsilon)^2$ versus low photon energy ($h\upsilon$) of ZnO (a), ZnO-MPS 2% (b), ZnO-MPS 5% (c) and ZnO-MPS 10% (d).

A comparative study of the emission properties of both unmodified and organosilane-modified ZnO materials was performed. Photoluminescence spectra of all samples, collected by irradiating them at 365 nm, are shown in Figure 8. Unmodified ZnO sample shows a wide emission band centered at *ca.* 578 nm, which is associated to electronic transitions of surface defects, such as zinc and oxygen vacancies, interstitial zinc and/or oxygen atoms.[39,40] The ZnO-MPS 2% material displays a much more intense emission band with respect to the unmodified one, with a maximum centered at *ca.* 556 nm. As the organosilane loading increases, a blue-shift and subsequent increase of the emission intensity is observed for the highest loaded ZnO-MPS 10% sample, showing the most intense emission band with the maximum centered at 546 nm. And also concerning the photoluminescence properties, the most important variation in relation to unmodified ZnO sample occurs at a 2% addition of MPS. The blue-shift of the emission bands can be related to a decrease of the particles size of MPS-modified ZnO samples, as already observed for organosilane-modified ZnO samples reported in the literature.[41,42]

On the other hand, functionalization of ZnO surface can also constitute an additional factor in triggering a further increase and/or modification of surface defects.[43,44] As a matter of fact, a certain type of electronic relaxation mainly causes such a broad emission band, in which surface O^{2-}/O^{-} states are trapping inside them the photogenerated holes. Through tunneling processes and subsequent recombination with oxygen vacancies, these trapped holes are able to return into the bulk phase. Consequently, this recombination promotes the emission effect in the visible domain, becoming more intense for the ZnO nanoparticles with smaller sizes.[45] In Figure 9 digital photographs of both unmodified ZnO and organosilane-modified ZnO powders, collected under UV irradiation at 365 nm, are shown. As expected, based on the above mentioned photoluminescence spectra, the unmodified ZnO sample shows the weakest emission, whereas ZnO-MPS 5% and ZnO-MPS 10% samples give the strongest emissions.

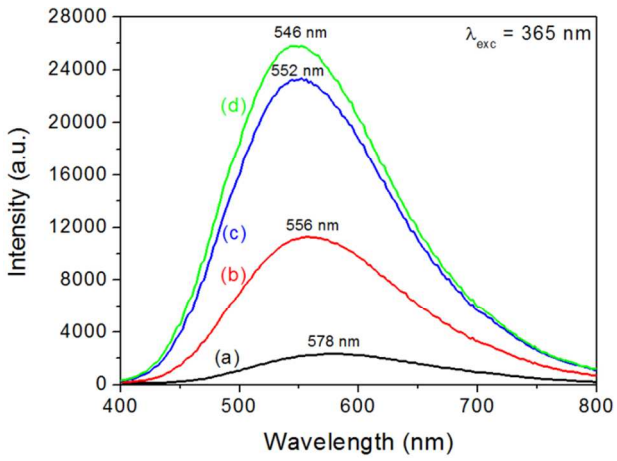

Figure 8. Solid state photoluminescence spectra of ZnO (a), ZnO-MPS 2% (b), ZnO-MPS 5% (c) and ZnO-MPS 10% (d) collected with an excitation wavelength of 365 nm.

In the light of these phenomena, surface modification of ZnO nanoparticles through functionalization with the MPS organosilane species can constitute an useful tool for tuning the photoluminescence efficiency and emission wavelength. Therefore, the organosilane surface functionalization during the growth process can significantly induce the reduction of the particles aggregation, thus promoting an augment of the number of effective surface luminescence centers.

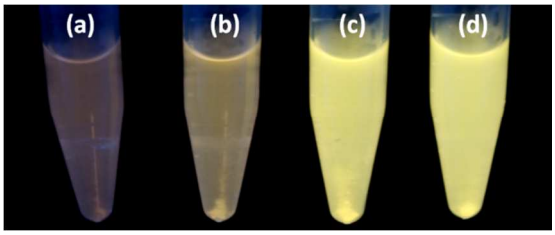

Figure 9. Digital photographs of ZnO (a), ZnO-MPS 2% (b), ZnO-MPS 5% (c) and ZnO-MPS 10% (d) powders dispersed in isopropanol under UV irradiation at 365 nm.

From the point of view of photoluminescence mechanism, it is assumed that electron transitions from the conduction band to a deep-trapped defect state triggers the visible emission. Generally, in literature it is also shown that as the size of ZnO nanoparticles

becomes smaller upon functionalization with organic surfactants, the bandgap energy increases due to quantum size effects.[10] To the best of our knowledge, no other report deals with the experimental determination of band gap energy for organo-modified ZnO nanoparticles, and only mention this idea as a generally accepted trend. As a matter of fact, our results regarding the determination of band gap values for unmodified ZnO and MPS-treated ZnO nanoparticles (see on Figure 7) were found to show for the first time the reverse: size reduction of MPS-grafted ZnO QDs brings decreased band gap energies (Figure 10). More in detail, in the case of ZnO nanoparticles grafted with MPS surfactant, containing in its structure oxygen atoms possessing free electrons in their lone pairs, two opposite effects take place at the level of ZnO electronic bands with increasing surfactant concentration: shrinking of both valence and conduction band due to the size decrease of ZnO nanoparticles, and bands enlargement determined by electron injection from the oxygen atoms (having the lone pairs) of MPS bound to the surface of ZnO nanoparticles, respectively.

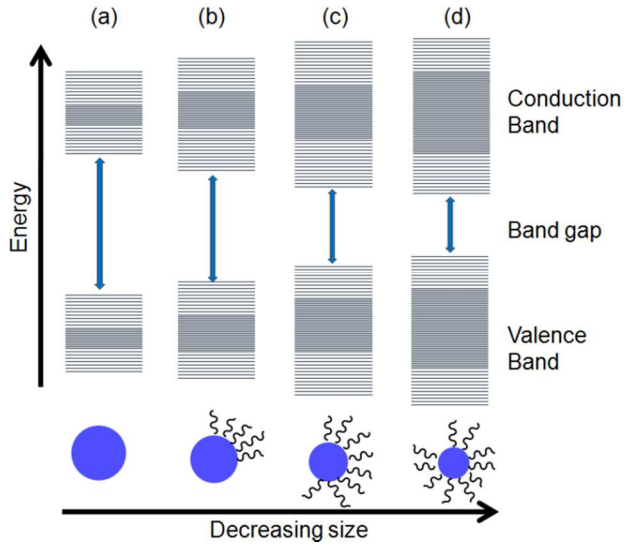

Figure 10. Schematic reppresentation of the band structures of ZnO (a), ZnO-MPS 2% (b), ZnO-MPS 5% (c) and ZnO-MPS 10% (d).

The dark areas in valence band and conduction band in Figure 10 represent a fine splitting of energy levels populated by the electrons injected from capping organosilanes. This splitting is due to the quantum confinement effect that is usually specific for quantum dots.[46]

Taking into account the decrease of band gap energies with the MPS concentration, it turns out that the bands enlargement by electron injection compensates and even overcomes the reduction effect of ZnO nanoparticles size. Silane coupling agents are known as external donors or electron donors. Literature data mention that the use of silane-coupling reagent for a strong chemical fixation of dye on, *e.g.*, TiO_2 nanoparticles, could enhance the electron injection into nanocristaline semiconductor particles, realizing the intramolecular energy transfer from highly absorbing chromophor groups, and subsequently improving the photosensitized efficiency.[47-50] The lifting of HOMO (highest occupied molecular orbital) level by incorporating donor ligands is one of the strategies successfully applied in designing sensitizers which absorb over the whole visible spectrum with application in dye-sensitized solar cells and sensitized photocatalysts for environmental purification.[47]

With the increase of surfactant concentration, due to nanoparticles size reduction, a limitation of the number of MPS molecules attached onto their surface takes place. This overlap of effects also explains the fact that the band gap reduction is not proportional with the surfactant concentration; this reduction is increasingly smaller at high concentration, that is, it is significant at the 2% MPS grafting and increasingly lower at higher MPS concentration of 5% and 10%, respectively. This unexpected situation brings a new insight into the relationship between the nanoparticle size reduction promoted by organic surfactant and the value of band gap energy. The close values of band gaps for the samples grafted with 5 and 10% organosilane, in correlation with the photoluminescence intensities, shows that a limitation of electron injection occurs. As a matter of fact, we have experimentally noticed that an organosilane loading more than 10% can no longer be attained, and therefore, the saturation limit of organosilane loading remains fixed at this percentage.

Conclusions

Hybrid organosilane-grafted ZnO quantum dots have been fabricated upon a successful surface attachement of 3-(trimethoxysilyl)propylmethacrylate (MPS) surfactant through a modified precipitation method, demonstrating remarkable hydrophobicity, high transmittance values and variable emission intensities in the visible domain under UV irradiation. A decrease of band gap energies, from 3.494 eV for unmodified ZnO to 3.377 eV for ZnO-MPS 10%, was detected. The 5% and 10% MPS-grafted ZnO nanoparticles displayed the best emission properties, constituting promissing candidates towards their implementation as active layers into hybrid light emitting device (HLED) for optoelectronic applications.

Acknowledgements

The work of Aurel Tăbăcaru has been funded by the Sectoral Operational Programme Human Resources Development 2007-2013 of the Ministry of European Funds through the Financial Agreement POSDRU/159/1.5/S/132397. Prof. Nicolae Tigau, Prof. Rodica Dinica, Dr. Mariana Busila and PhD student Viorica Ghisman from the "Dunărea de Jos" University of Galati (Romania) as well as PhD student Nertil Xhaferaj and Prof. Claudio Pettinari from the University of Camerino (Italy) are gratefully acknowledged for helpful experimental assistance and discussions.

Notes and references

[a] *Center of Nanostructures and Functional Materials – CNMF, Faculty of Engineering, "Dunărea de Jos" University of Galati, 111 Domneasca Street, 800201, Galați, Romania.*
E-mail: viorica.musat@ugal.ro; Tel. +40-757070613.
[b] *University Politehnica of Bucharest, Faculty of Applied Chemistry and Materials Science, Department of Science and Engineering of Oxide Materials and Nanomaterials, Polizu Street No. 1-7, 011061, Bucharest, Romania.*

† Electronic Supplementary Information (ESI) available: Synthesis of ZnO nanoparticles, crystallografic data, electron diffraction patterns, infrared spectrum of free MPS, reaction schemes for MPS grafting of ZnO nanoparticles, and table containing their stoichiometric formulations. See DOI: 10.1039/b000000x/

‡ Footnotes should appear here. These might include comments relevant to but not central to the matter under discussion, limited experimental and spectral data, and crystallographic data.

1 U. Ozgur, Ya. I. Alivov, C. Liu, A. Teke, M. A. Reshchikov, S. Dogan, V. Avrutin, S.-J. Cho, H. Morkoc, *J. Appl. Phys.* 2005, **98**, 041301.

2 J. Mawyin, Y. Shupyk, M. Wang, G. Poize, P. Atienzar, T. Ishwara, J. R. Durrant, J. Nelson, D. Kanehira, N. Yoshimoto, C. Martini, E. Shilova, P. Secondo, H. Brisset, F. Fages, J. Ackermann, *J. Phys. Chem. C* 2011, **115**, 10881.

3 E. Fortunato, P. Barquinha, R. Martins, *Adv. Mater.* 2012, **24**, 2945.

4 M. Karimi, J. Saydi, M. Mahmoodi, J. Seidi, M. Ezzati, S. Shamsi Anari, B. Ghasemian, *J. Phys. Chem. Solid* 2013, **74**, 1392.

5 Y. Martynova, B.-H. Liu, M. E. McBriarty, I. M. N. Groot, M. J. Bedzyk, S. Shaikhutdinov, H.-J. Freund, *J. Catal.* 2013, **301**, 227.

6 X. Tang, E. S. G. Choo, L. Li, J. Ding, J. Xue, *Langmuir* 2009, **25**, 5271.

7 D. M. Yebra, S. Kiil, C. E. Weinell, K. Dam-Johansen, *Prog. Org. Coat.* 2006, **56**, 327.

8 M. Ibanescu (Busila), V. Musat, T. Textor, V. Badilita, B. Mahltig, *J. Alloys Comp.* 2014, **610**, 244.

9 M. Monge, M. L. Kahn, A. Maisonnat, B. Chaudret, *Angew. Chem. Int. Ed.* 2003, **42**, 5321.

10 N. S. Pesika, Z. Hu, K. J. Stebe, P. C. Searson, *J. Phys. Chem. B* 2002, **106**, 6985.

11 S. Tachikawa, A. Noguchi, T. Tsuge, M. Hara, O. Odawara, H. Wada, *Materials* 2011, **4**, 1132.

12 A. Aboulaich, C.-M. Tilmaciu, C. Merlin, C. Mercier, H. Guilloteau, G. Medjahdi, R. Schneider, *Nanotechnology* 2012, **23**, 335101.

13 M. Kotecha, W. Veeman, B. Rohe, M. Tausch, *Micropor. Mesopor. Mater.* 2006, **95**, 66.

14 C. Bressy, V. G. Ngo, F. Ziarelli, A. Margaillan, *Langmuir* 2012, **28**, 3290.

15 H.-C. Huang, T.-E. Hsieh, *Ceramics International* 2010, **36**, 1245.

16 Z. Guo, S. Wei, B. Shedd, R. Scaffaro, T. Pereira, H. T. Hann, *J. Mater. Chem.* 2007, **17**, 806.

17 R. Ciriminna, A. Fidalgo, V. Pandarus, F. Beland, L. M. Ilharco, M. Pagliaro, *Chem. Rev.* 2013, **113**, 6592.

18 O. S. Heavens, Optical properties of thin solid films, Butterworths, London: 1955.

19 E. Shanti, E. Dutta, A. Banerjee, K. L. Chopra, *J. Appl. Phys.* 1981, **51**, 6243.

20 D. Bhattacharyya, S. Chaudhuri, A. K. Pal, *Vacuum* 1992, **43**, 313.

21 V. Srikant, D. R. Clarke, *J. Appl. Phys.* 1997, **81**, 6357.

22 S. T. Tan, B. J. Chen, X. W. Sun, W. J. Fan, H. S. Kwok, X. H. Zhang, S. J. Chua, *J. Appl. Phys.* 2005, **98**, 013505.

23 T. Prasada Rao, M. C. Santhoshkumar, *Appl. Surf. Sci.* 2009, **255**, 4579.

24 N. Ghraïri, F. Aousgi, M. Zribi, M. Kanzari, *Calchogenide Letters* 2010, **7**, 217.

25 M. Mazhdi, P. Hossein Khani, *Int. J. Nano Dim.* 2012, **2**, 233.

26 D. K. Schroeder, Semiconductor materials and device characterisation, Wiley: 1990.

27 J. F. Muth, J. H. Lee, I. K. Shmagin, R. M. Kolbas, H. C. Casey, B. P. Keller, U. K. Mishra, S. P. DenBaars, *Appl. Phys. Lett.* 1997, **71**, 2572.

28 C. H. Huang, G. Zhang, Z. Q. Chen, X. J. Huang, H. Y. Shen, *Optics and Laser Technology* 2002, **34**, 209.

29 V. Pena-Mendez, M. T. S. Nair, P. K. Nair, *Semicond. Sci. Technol.* 2006, **21**, 450.

30 K. L. Chopra, Thin Film Phenomena. McGraw-Hill, New York, 1969.

31 R. Brayner, S. A. Dahoumane, C. Yepremian, C. Djediat, M. Meyer, A. Coute, F. Fievet, *Langmuir* 2010, **26**, 6522.

32 A. L. Patterson, *Phys. Rev.* 1939, **56**, 972.

33 K. Nakamoto, Infrared and Raman spectra of inorganic and coordination compounds, Part B, 6th Edition, Wiley: 2009.

34 E. Tang, H. Liu, L. M. Sun, E. Zheng, G. X. Cheng, *Eur. Polym. J.* 2007, **43**, 4210.

35 L. Hiltunen, M. Leskelä, M. Mäkelä, L. Niinistö, *Acta Chem. Scand.* 1987, **A41**, 548.

36 V. Musat, P. Budrugeac, C. Gheorghies, *J. Therm. Anal. Cal.* 2008, **94**, 373.

37 A. H. Moharram, S. A. Mansour, M. A. Hussein, M. Rashad, *J. Nanomaterials* 2014, 716210.

38 F. K. Shan, Y. S. Yu, *J. Eur. Ceram. Soc.* 2004, **24**, 1869.

39 K. Vanheusden, W. L. Warren, C. H. Seager, D. R. Tallant, J. A. Vogit, B. E. Gnade, *J. Appl. Phys.* 1996, **79**, 7983.

40 M. K. Patra, M. Manoth, V. K. Singh, G. Siddaramana Gowd, V. S. Choudhry, S. R. Vadera, N. Kumar, *Journal of Luminescence* 2009, **129**, 320.

41 H.-Q. Shi, W.-N. Li, L.-W. Sun, Y. Liu, H.-M. Xiao, S.-Y. Fu, *Chem. Commun.* 2011, **47**, 11921.

42 D. Costenaro, F. Carniato, G. Gatti, L. Marchese, C. Bisio, *New J. Chem.* 2013, **37**, 2103.

43 L. Guo, S. Yang, C. Yang, P. Yu, J. Wang, W. Ge, G. K. L. Wong, *Appl. Phys. Lett.* 2000, **76**, 2901.

44 K. Borgohain, S. Mahamuni, *Semicond. Sci. Technol.* 1998, **13**, 1154.

45 A. van Dijken, E. A. Meulenkamp, D. Vanmaekelbergh, A. Meijerink, *Journal of Luminescence* 2000, **87-89**, 454.

46 S. M. Reimann, M. Manninen, *Revs. Modern Phys.* 2002, **74**, 1283.

47 D. Pei, J. Luan, *Int. J. Photoenergy* 2012, 262831.

48 F. Liu, G. J. Meyer, *Inorg. Chem.* 2005, **44**, 9305.

49 Y. S. Chen, C. Li, C. H. Zheng, W. B. Wang, X. S. Wang, B. W. Zhang, *J. Mater. Chem.* 2005, **15**, 1654.

50 T. Peng, K. Dai, H. Yi, D. Ke, P. Cai, L. Zan, *Chem. Phys. Lett.* 2008, **460**, 216.